

Independent Light Field Manipulation in Diffraction Orders of Metasurface Holography

Xin Li,* Xue Zhang, Ruizhe Zhao, Guangzhou Geng, Junjie Li, Lingling Huang,* and Yongtian Wang*

Metasurface holograms are novel optical elements with enormous potential because of the charming electromagnetic features, which can manipulate amplitude, phase, polarization state, and other parameters of light field via an elaborately designed subwavelength nanostructure array. Metagratings are extensively researched for controlling the feature of light in diffraction orders. However, a flexible and simple method is yearned for realizing independent wavefront manipulation in different orders. Here, a metasurface holography that can reconstruct various information in each diffraction order is demonstrated. The physical model is based on Jacobi–Anger expansion and iterative optimization, and both helicity-dependent and birefringent metasurfaces can work compatibly with this proposed method to achieve arbitrary control of 1D and 2D orders. Specifically, information in 18 channels consisting of diffraction orders and polarization states is encoded in a single metasurface hologram. The approach provides promising and versatile optical elements for beam shaping, holographic display, optical storage, information encryption, etc.

1. Introduction

High-performance novel flat optical elements are earnestly demanded for various minimized and integrated applications in recent years. Optical metasurface is a kind of promising elements composed of delicately designed artificial subwavelength nanostructures, which is termed metaatoms. Because of the strong interaction between metaatoms and light, these ultrathin and versatile optical elements have incredible power to manipulate the parameters of light field.^[1–5] Introducing holography can further expand the flexibility, especially the multiplexing technologies of


metasurface holography bring vitality to the development and applications of such platform. Benefited from these multiplexing technologies, more functions are able to be embedded in a single metasurface via the multiple manipulation channels of phase, amplitude, polarization, frequency, orbit angular momentum, incident angle, and so on.^[6–15]

Metasurfaces own the function of beam folding and splitting, such as being applied in the generation of cold atoms,^[16] while it can achieve more than that, which enable steer the parameters (including amplitude, phase, polarization, and even quantum states of photons) of specific orders via proper design: the resonant mode of nanostructures boosted the generation of uniform diffraction efficiency of desired orders;^[17–20] the reconfigurable structure led to tunable diffraction directions;^[21] a

metagrating array was demonstrated to achieve multiphoton quantum state measurement and reconstruction;^[22] an optimization method based on anisotropy of metaatom or spatial multiplexing made Stokes parameters measurable, and compact full-Stokes polarization cameras could be realized.^[23,24] Nevertheless, previously reported metasurfaces can only uniformly manipulate the parameters in each order and Damman gratings offer extra opportunities to generate more complicated light field distributions through phase or transmission coefficient optimization.^[25,26] Introducing Damman gratings to metasurface holography improves the reconstructed images qualities,^[27,28] and further the Bessel beam and Airy beam array were formed.^[29–31] Meanwhile the optimization methods of Damman gratings achieved the generation of vertex beam arrays with different topological charges in each order by both traditional light modulators and metasurfaces.^[32] However, for a phase grating, it is easy to learn that the series expansion of grating function indicates a commonly general relationship between each order, hence more complex wavefront distributions in each order in far field can be obtained by applying superposition of complex amplitude and complicated optimization algorithms according to above methods. An effort on nanostructure design had also been made,^[33] where a supercell library was built and the position of supercells was also involved in the optimization for realize a flexible manipulation in each order, but somehow such supercell structures brought asymmetric and bigger unit size and

X. Li, X. Zhang, R. Zhao, L. Huang, Y. Wang
Beijing Engineering Research Center of Mixed Reality and Advanced Display
School of Optics and Photonics
Beijing Institute of Technology
Beijing 100081, China
E-mail: lix@bit.edu.cn; huanglingling@bit.edu.cn; wyt@bit.edu.cn

G. Geng, J. Li
Beijing National Laboratory for Condensed Matter Physics
Institute of Physics
Chinese Academy of Sciences
Beijing 100191, China

 The ORCID identification number(s) for the author(s) of this article can be found under <https://doi.org/10.1002/lpor.202100592>

DOI: 10.1002/lpor.202100592

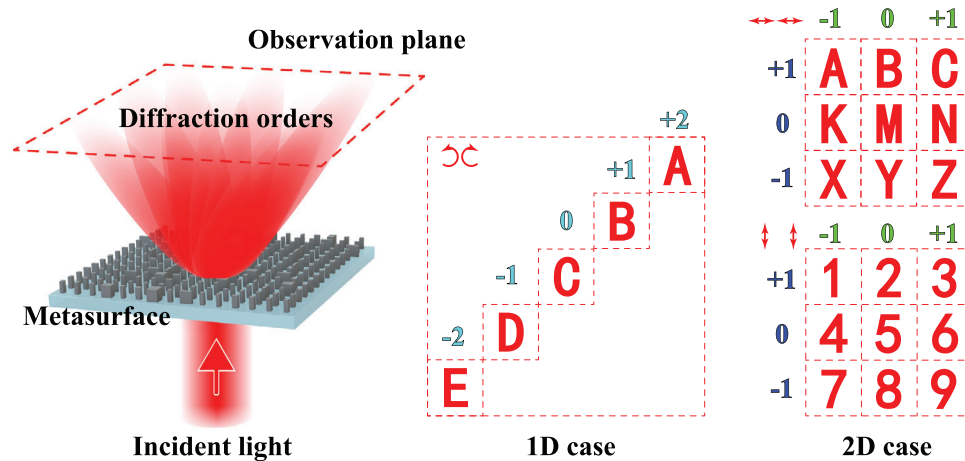


Figure 1. Schematic of light field manipulation in diffraction orders of metasurface holography. The arrows indicate the polarization states of the incident and emission light. The dashed area represents effective area on imaging plane. For 1D case, cyan numbers represent the orders; for 2D case, green and blue numbers are the orders along horizontal and vertical axis, respectively.

increased the difficulty of metasurface design. Consequently, a desired method for arbitrarily manipulating the light field in far field should be simpler, meanwhile the commonly general relationship can be restricted on metasurface only, which will not limit the far-field behavior. Apparently, this method would extend the potential applications of metasurfaces.

Here, we propose and demonstrate a kind of metasurface holography that the light field of each order can be manipulated independently in far field. We design helicity-dependent and birefringent metasurfaces by encoding a series of images in both 1D and 2D orders via an optimization method, which is developed based on Jacobi–Anger expansion and Fidoc algorithm. In the experimental verifications, both helicity-dependent and birefringent metasurfaces work well, and independent images in 3×3 diffraction orders and two orthogonal polarization channels are reconstructed successfully. This metasurface holography renders a novel way to simultaneously and independently modulate the amplitude and diffraction orders of light. Integrated with other type of multiplexing, this approach can provide another manipulation dimension and applied to various fields of optics and photonics, such as beam shaping, information display, data storage, and optical encryption.

2. Results

A schematic of independent wavefront manipulation in diffraction orders is shown in **Figure 1**. For the purpose, the metasurface encoded with holographic information (metasurface hologram), is delicately designed. In 1D case, a primary phase-only hologram $\exp[i\varphi(x, y)]$ is reencoded as

$$E(x, y) = \exp \left\{ j\beta \left\{ \cos \left[\varphi(x, y) - \varphi_r(x, y) \right] + \varphi_0(x, y) \right\} \right\} \quad (1)$$

where β is the coefficient for amplitude manipulation of each order, j is imaginary number, $\varphi_0(x, y)$ is initial phase, and $\varphi_r(x, y)$ is basic reference phase defining the diffraction orders. Then this expression can be expanded as the sum of each order according

to Jacobi–Anger expansion,^[34] and the m order is written as

$$E^{(m)}(x, y) = j^m J_m(\beta) \exp \left\{ j \left[m\varphi(x, y) + \varphi_0(x, y) \right] \right\} \exp \left[jm\varphi_r(x, y) \right] \quad (2)$$

where $J_m(*)$ is the m order of the Bessel function of the first kind. Then it is obvious that the complex wavefront of each order relies on the reconstruction of $J_m(\beta) \exp\{j[m\varphi(x, y) + \varphi_0(x, y)]\}$. To realize these complex amplitude distributions expressing different information, the primary hologram should be elaborately designed. The reference phase is satisfied with $\varphi_r(x, y) = k[x \sin \theta_x + y \sin \theta_y]$, where θ_x and θ_y are the diffraction angles of the first order along two directions, respectively. When the incident beam is illuminated on the metasurface hologram, the target images for each order are reconstructed on observation plane (k -space in our verifications). The flowchart of computer-generated hologram (CGH) encoding process is shown in **Figure 2** and there are three main steps. In step 1, $\varphi_0(x, y)$ is obtained based on original Fidoc algorithm.^[35] In step 2, another iterative process is performed: the target amplitude information is modified based on Fidoc algorithm, and divided by $\exp[i\varphi_0(x, y)]$ after the inverse propagation (it is inverse Fourier transformation in our verifications, but it could be others like inverse Fresnel diffraction or inverse angular spectrum propagation); before carrying out weighted sum, a phase unification process is introduced (for details about this phase unification process, see Part A, Supporting Information); one can acquire a phase-only hologram $\exp[i\varphi(x, y)]$ via ignoring the amplitude of the weighted sum; the phase is multiplied the times N_1 to N_n in each order respectively, which is then multiplied by $\exp[i\varphi_0(x, y)]$; then a group of complex amplitude distributions is obtained after the forward propagation (Fourier transformation in our work) for the reconstruction quality evolution and also for amplitude modifications in next iteration loop. When the quality meets the requirement or the iteration exceeds upper limit, the second iterative process can be terminated and the primary phase-only hologram is input to the final step. In step 3, the primary hologram, $\varphi_0(x, y)$, and $\varphi_r(x, y)$

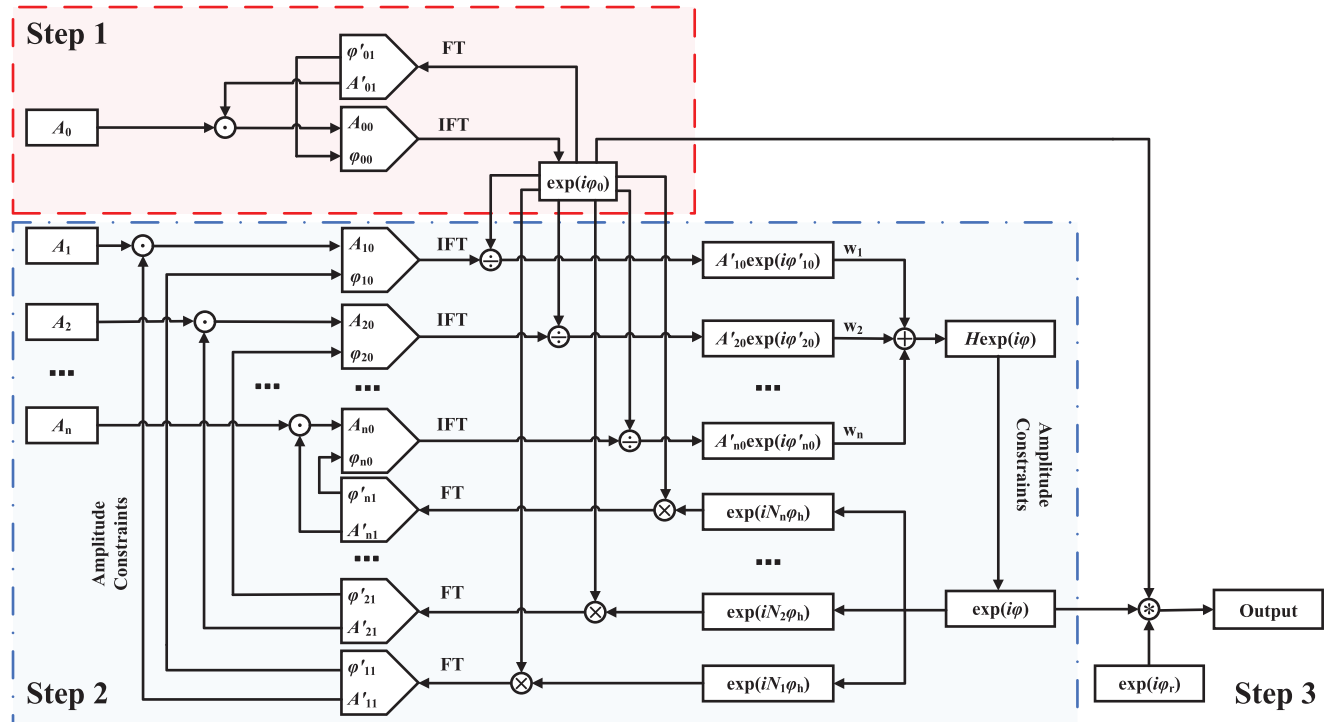


Figure 2. Flow chart of iterative optimization algorithm for light field manipulation in diffraction orders. IFT and FT are inverse Fourier transformation and Fourier transformation, respectively. “.” in circle represents amplitude constraints based on Fidoc algorithm, “×” and “÷” means multiplying and dividing, respectively, “+” is weighted sum after phase unification process, and “*” indicates mapping based on Equation (1) or (3).

are encoded as final CGH according to Equation (1). After the weighted sum, there is an amplitude unification process to guarantee the energy conservation.

This method can also be generalized to 2D manipulation, and the CGH is reencoded as

$$E(x, y) = \exp \left\{ j \left[\alpha \cos [a\varphi(x, y) - \varphi_{rx}(x, y)] + \beta \cos [b\varphi(x, y) - \varphi_{ry}(x, y)] + \varphi_0(x, y) \right] \right\} \quad (3)$$

where $\varphi_{rx}(x, y) = kx \sin \theta_x$ and $\varphi_{ry}(x, y) = ky \sin \theta_y$ are used to define the diffraction orders, α and β are coefficients for amplitude manipulation (they can be any positive real numbers), respectively, and a and b are control parameters for determining the multiple of $\varphi(x, y)$ in each order (they should be integers). Then Equation (3) is expanded as

$$E(x, y) = \sum_n \sum_m J_m^{m+n}(\alpha) J_n(\beta) \exp \left\{ j [(am + bn)\varphi(x, y) + \varphi_0(x, y)] \right\} \exp [j\varphi_{xy, mn}(x, y)] \quad (4)$$

where $\varphi_{xy, mn}(x, y) = k[mx \sin \theta_x + ny \sin \theta_y]$. It is shown that the information of light field manipulation in each order is encoded as $[(am + bn)\varphi(x, y) + \varphi_0(x, y)]$. For instance, in our verification, we focus on the nine orders (3×3) in the Fourier plane and set $a = 3$, $b = 1$ (for details about control parameters and diffraction

orders, see Part B, Supporting Information), and the different multiples of $\varphi(x, y)$ are as follows

$$\begin{bmatrix} -2 & 1 & 4 \\ -3 & 0 & 3 \\ -4 & -1 & 2 \end{bmatrix} \quad (5)$$

While the phase modulation in central order can be achieved by $\varphi_0(x, y)$. Then, by the iterative optimization algorithm, different information can be encoded into each order as a CGH. α and β determine the intensity contrast of each order according to the order of first kind of Bessel function as shown in Figure 3a and for details about this phase unification process, see Part C in the Supporting Information. Moreover, the CGHs for 1D and 2D manipulations are shown in Figure 3b,c.

To verify the compatibility of proposed method, we design a helicity-dependent and a birefringent metasurface to achieve one and two polarization channels multiplexing. In the design of former one, Pancharatnam–Berry (PB) phase is utilized, and for latter one, propagation phase is applied. As shown in Figure 3d, the metasurface hologram consists of rectangular amorphous silicon nanorod arrays on glass substrate. A rigorous coupled wave analysis method is applied to aid the design of metaatom. For a similar experiment condition, the period of both helicity-dependent and birefringent metasurfaces are set as 280 nm and the height of nanorods is 600 nm. During the design, we sweep the width and length of nanostructure to acquire a library of structures, as shown in Figure 3e,f (for details see Part C, Supporting Information). The optimized size of each rod on birefringent metasurface

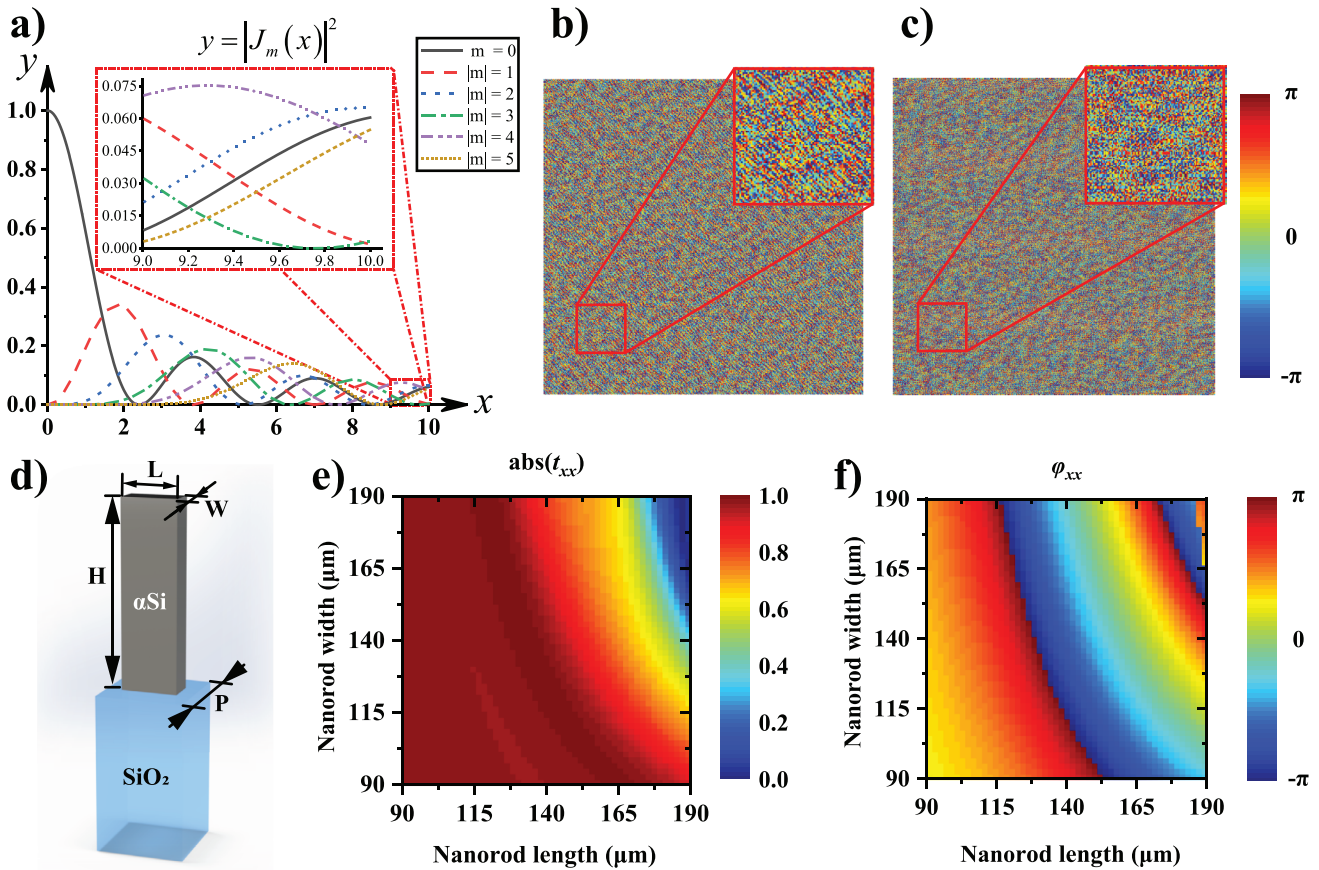


Figure 3. Design of diffraction order manipulation metasurface holography. (a) is selection impact of the coefficient for amplitude manipulation. The solid line, dash line, dotted line, dotted-dashed line, double dotted-dashed line, and double dotted line represent the absolute value of the orders of the Bessel function from 0 to 5. The independent variables x are the coefficient for amplitude manipulation of each order and the dependent variable y defines the intensities of each order according to Equations (2) and (4). (b) and (c) are the CGHs for 1D and 2D manipulation, respectively, where zoom-in view of them are given. (d) is the schematic illustration of the metaatom. (e) and (f) are simulated amplitude and phase of the transmission coefficients t_{xx} of amorphous silicon nanorods on silica by a rigorous coupled wave analysis method for parameters optimizations. The sweeping length and width of nanorods are both from 90 to 190 nm at the incident wavelength of 800 nm.

is selected to obtain the minimized phase difference between the target values and calculated values in both channels. While the size on helicity-dependent metasurface is picked out where the metaatom performs as a half-wave plate and the rotation angle of each rod determined by the CGH according to the principle of PB phase.

The experiments are performed to verify the feasibilities of our proposed method. The scanning electron microscopy results of helicity-dependent sample and birefringent one are shown in Figure 4a–d, respectively. The setup is exhibited in Figure 4e. The incident light passes through polarization optical elements and is collimated on the metasurface by a lens; then the emitted beams are collected by an objective and a lens, and finally imaged on a charge coupled device (CCD) camera after a lens and polarization optical element(s). The scalar simulation and experimental results are shown in Figure 5, where Sample 1 and Sample 2 are helicity-dependent and birefringent metasurfaces, respectively. It is worth noting that all simulation results are obtained based on scalar diffraction theory. For helicity-dependent metasurface the polarization of incident light is right circular polarization (RCP)

and observation polarization is left circular polarization (LCP) as marked in Figure 5d. For birefringent samples, in Figure 5e, the incident and observation polarization are horizontal, and in Figure 5f, they are both vertical. The appropriate rotation angles of polarization optical elements ensure that the light with correct polarization states is incident on the metasurfaces, and different holographic images are reconstructed in the desired diffraction orders successfully. By optimization of the control parameters, the coefficients for amplitude manipulation and weights in encoding process, the intensities of each order can be tuned arbitrarily: the intensities of each order can be similar with each other as the result for helicity-dependent metasurface shown in Figure 5d, or they can be different as in the results for birefringent samples exhibited in Figure 5e,f. The functions of proposed metasurface holography are not limited at single working wavelength, and changing the wavelength of the incident light can also lead to successful reconstructions. We use the illumination light with the wavelength from 700 to 900 nm, and some results are exhibited in Figure S4 in the Supporting Information. Furthermore, the basic principle of helicity-dependent and birefringent

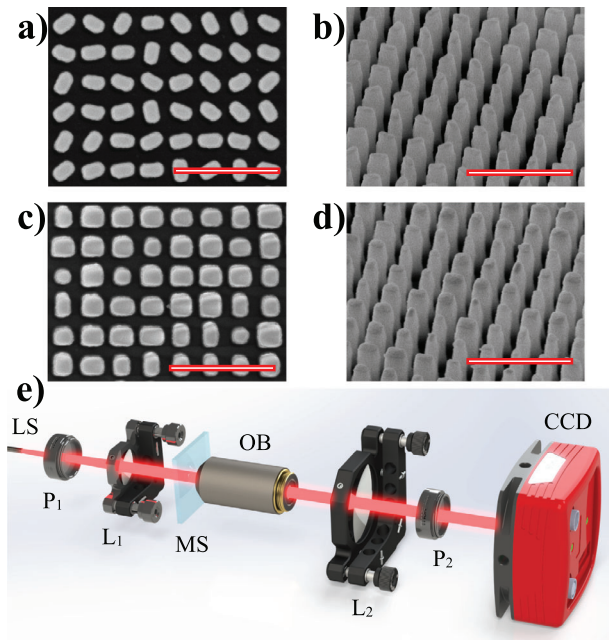


Figure 4. Experimental verification of independent manipulation in diffraction orders. (a) and (b) Scanning electron microscopy images of the fabricated helicity-dependent metasurfaces metasurface sample and (c) and (d) are that of the birefringent sample. The scale bars in (a)–(d) are 1 μm . e) Experimental verification setup. LS, the supercontinuum laser source; L_1 and L_2 , convex lenses; OB, objective lens; P_1 and P_2 , polarization optical elements; MS, metasurface; CCD, charge coupled device.

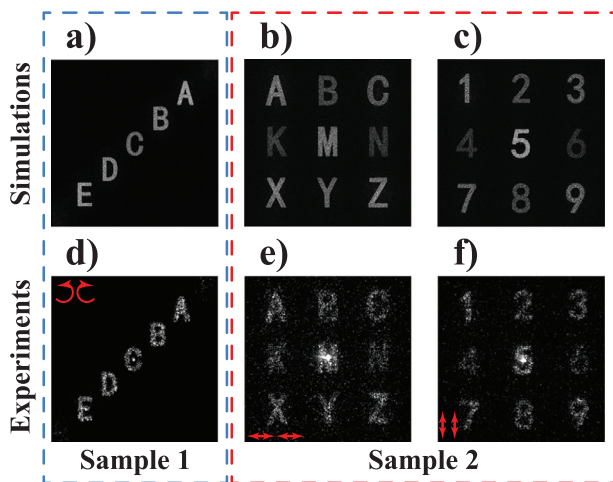


Figure 5. Simulation and experimental results for independent light field manipulation in diffraction orders of metasurface holography. a–c) Simulation results for 1D and 2D cases. d–f) Corresponding experimental results, where the arrows represent the polarization states of the incident and emission light.

metasurfaces offer broadband properties, and the details are discussed in Part D in the Supporting Information.

3. Discussions

The intensity contrast between each order can be manipulated via modifying the parameters α and β in Equations (2) and (4),

and the weight w_1 to w_n in encoding process. As described in Equations (2) and (4), amplitude manipulation coefficients (in 1D case $\alpha=2.95$ and in 2D case $\alpha = \beta = 1.65$) determine the intensity of each order. Meanwhile the feature of Bessel function of first kind $|J_{-m}(\alpha)| = |J_m(\alpha)|$ indicates the intensity of $-m$ order is equal to that of m order, which also can be learnt from the results. Growth of independent variable leads to a smaller difference between each order of Bessel functions, which means that bigger α and β would be easier to get a smaller intensity contrast; however, the absolute value of Bessel functions goes smaller, which indicates the efficiencies of each order will be much lower (for more discussion, see Part C, Supporting Information). Also, the introduction of weight w_1 to w_n enables to artificially modulate the intensity contrast between each order. It is worth noting that because both the phase unification and amplitude constraint on metasurface plane are nonlinear process, the weight cannot be set only according to desired intensities contrast, but it should be in direct proportion to the contrast. Consequently, we set $w_1 = w_{-1} = w_2 = w_{-2} = 1$ in our 1D case for same intensities in each order, while $w_1 = w_{-1} = \dots = w_1 = w_{-3} = 1, w_4 = w_{-4} = 3$ for similar intensities. These weight coefficients are bigger than 1, owing to the suppress of undesired orders in the optimization, and the energy conservation can be guaranteed for there is an amplitude constraint after the weighted sum.

In helicity-dependent case, although most RCP light is converted to LCP, there is little RCP that is not converted because of the geometric deviation and mismatch of permittivity between design and practical fabrication. Limited by the extinction ratio of polarizer, there is some unconverted light focused in the center of the imaging plane as a bright spot. While for the birefringent metasurface this deviation and mismatch, and the coherent speckle lead to a strong background noise. These issues also decay the image qualities in the reconstruction for propagation phase case and the image qualities deteriorate a bit for the target images are reconstructed with the same polarization state as incident light.

Inspired by Shannon–Hartley theorem, the total information capacity I_c of a light field can be described as^[36–38]

$$I_c = N_{\text{DoF}} \log_2(1 + \text{SNR}) \quad (6)$$

where N_{DoF} is the total degrees of freedom (DoF) and SNR is the signal-to-noise ratio. Further, $N_{\text{DoF}} = N_t N_s N_f N_p$, here N_t , N_s , N_f , and N_p are the temporal, spatial, frequency, and polarization DoF,^[37] which are all integers. In the independent light field manipulation in diffraction orders, $N_t = N_f = 1$, and $N_p = 1$ when PB phase is applied, $N_p = 2$ for the birefringent situation. No matter which methods are applied to the design of metasurface holograms, Equation (6) determines the maximum information capacity. It is apparent that higher information capacity brings better effect of light field manipulation. For most conventional methods, the manipulation information should be optimized globally, and $N_s = XY$, where X and Y are the spatial-bandwidth-product along x axis and y axis. As for our proposed method, all target manipulation information is optimized locally, which is concentrated around each order, and the total spatial DoF $N'_s = \sum_{m,n} X_{(m,n)} Y_{(m,n)} < N_s$. This indicates that if less arguments are involved in the optimization, and it would decrease the difficulty of this process and lead to a better manipulation qual-

ity. For further enhancing the light field manipulation of metasurface holography, an effective way is increasing the DoF according to Equation (6), such as applying more complicated structure of metaatom, or specific working mode of nanostructure.^[39–40]

4. Conclusion

In conclusion, the method reported herein can fully combine the advantages of CGH and optical metasurface to realize independent light field manipulation in diffraction orders. The commonly general relationship between each diffraction order is released by our proposed iterative method based on Jacobi–Anger expansion and Fidoc algorithm and by combining with smart algorithm, this approach offers several parameters in optimization process to modify the holographic intensity distribution of each order. The target light field are reconstructed successfully in simulation and experimental verifications, which exhibit that both helicity dependent and birefringent metasurfaces support 1D and 2D diffraction orders control. Nevertheless, it does not mean that this method can only work with these two kinds of metasurface. Our approach is compatible with most multiplexing metasurface holography and the increase of information recorded in metasurface hologram by using diffraction orders brings much more manipulation channels. This study of diffraction orders as different multiplexing channels leads to another dimension for information storage, display, encryption, and other complex light field manipulations.

5. Experimental Section

In the experimental verifications, a supercontinuum laser source, NKT Photonics Superk EVO, is applied as the light source, while Thorlabs 1501C-USB is used for capturing reconstruction results. P_1 and P_2 are employed for the generation and analysis of polarization state. For helicity-dependent case, P_1 is a group of the polarization optical elements consisting of a polarizer and a quarter wave plate for circular polarization generation, and P_2 are a quarter wave plate and an analyzer to filter out copolarization beam without carrying phase information. For birefringent case, the polarization optical elements P_1 are a polarizer and a half wave plate and P_2 is an analyzer only.

Supporting Information

Supporting Information is available from the Wiley Online Library or from the author.

Acknowledgements

The authors acknowledge the funding provided by the National Key R&D Program of China (2021YFA1401200), Beijing Outstanding Young Scientist Program (BJJWZYJH01201910007022), National Natural Science Foundation of China (Nos. U21A20140 and 92050117) program, Fok Ying-Tong Education Foundation of China (No. 161009), and Beijing Municipal Science and Technology Commission, Administrative Commission of Zhongguancun Science Park (No. Z211100004821009). X.L. acknowledges the support from Beijing Institute of Technology Research Fund Program for Young Scholars (XSQD-201904005).

Authors Contribution

X.L. proposed the original idea, X.L., X.Z., and L.H. improved the idea, X.L. and L.H. performed metasurface designs and numerical simulations,

G.G. and J.L. fabricated the sample, X.L., R.Z., G.G., and J.L. carried out the measurements, X.L., X.Z., R.Z., L.H., and Y.W. prepared the paper, and L.H. and Y.W. supervised the overall project. All of the authors analyzed the data and discussed the results.

Conflict of Interest

The authors declare no conflict of interest.

Data Availability Statement

The data that support the findings of this study are available from the corresponding author upon reasonable request.

Keywords

diffraction orders, holography, light field manipulation, metasurfaces

Received: October 19, 2021

Revised: February 4, 2022

Published online: May 19, 2022

- [1] C.-W. Qiu, W. Jiang, T. Cui, *Sci. Bull.* **2019**, *64*, 791.
- [2] X. Li, X. Ma, X. Luo, *Opto-Electron. Eng.* **2017**, *44*, 255.
- [3] A. H. Dorrah, N. A. Rubin, A. Zaidi, M. Tamagnone, F. Capasso, *Nat. Photonics* **2021**, *15*, 287.
- [4] Z. Yin, Y. Shi, M. Cen, T. Cao, C. Xu, D. Luo, G. Li, Y.-J. Liu, *Sci. Bull.* **2021**, *66*, 1518.
- [5] M. Decker, I. Staude, M. Falkner, J. Dominguez, D. N. Neshev, I. Brener, T. Pertsch, Y. S. Kivshar, *Adv. Opt. Mater.* **2015**, *3*, 813.
- [6] Y. Bao, L. Wen, Q. Chen, C.-W. Qiu, B. Li, *Sci. Adv.* **2021**, *7*, eabh0365.
- [7] P. Zheng, Q. Dai, Z. Li, Z. Ye, J. Xiong, H.-C. Liu, G. Zheng, S. Zhang, *Sci. Adv.* **2021**, *7*, eabg0363.
- [8] I. Kim, W.-S. Kim, K. Kim, M. A. Ansari, M. Q. Mehmood, T. Badloe, Y. Kim, J. Gwak, H. Lee, Y.-K. Kim, *Sci. Adv.* **2021**, *7*, eabe9943.
- [9] H. Ren, X. Fang, J. Jang, J. Bürger, J. Rho, S. A. Maier, *Nat. Nanotechnol.* **2020**, *15*, 948.
- [10] X. Fang, H. Ren, M. Gu, *Nat. Photonics* **2020**, *14*, 102.
- [11] L. Deng, J. Deng, Z. Guan, J. Tao, Y. Chen, Y. Yang, D. Zhang, J. Tang, Z. Li, *Light: Sci. Appl.* **2020**, *9*, 101.
- [12] E. Wang, J. Niu, Y. Liang, H. Li, Y. Hua, L. Shi, C. Xie, *Adv. Opt. Mater.* **2020**, *8*, 1901674.
- [13] S. C. Malek, H.-S. Ee, R. Agarwal, *Nano Lett.* **2017**, *17*, 3641.
- [14] E. Almeida, O. Bitton, Y. Prior, *Nat. Commun.* **2016**, *7*, 12533.
- [15] L. Jin, Y.-W. Huang, Z. Jin, R. C. Devlin, Z. Dong, S. Mei, M. Jiang, W. T. Chen, Z. Wei, H. Liu, *Nat. Commun.* **2019**, *10*, 4789.
- [16] L. Zhu, X. Liu, B. Sain, M. Wang, C. Schlickriede, Y. Tang, J. Deng, K. Li, J. Yang, M. Holynski, *Sci. Adv.* **2020**, *6*, eabb6667.
- [17] Y. Ra'di, D. L. Sounas, A. Alù, *Phys. Rev. Lett.* **2017**, *119*, 067404.
- [18] Z. Fan, M. R. Shcherbakov, M. Allen, J. Allen, B. Wenner, G. Shvets, *ACS Photonics* **2018**, *5*, 4303.
- [19] Z. Zhang, M. Kang, X. Zhang, X. Feng, Y. Xu, X. Chen, H. Zhang, Q. Xu, Z. Tian, W. Zhang, *Adv. Mater.* **2020**, *32*, 2002341.
- [20] T. Shi, Y. Wang, Z. L. Deng, X. Ye, Z. Dai, Y. Cao, B. O. Guan, S. Xiao, X. Li, *Adv. Opt. Mater.* **2019**, *7*, 1901389.
- [21] Y. Ra'di, A. Alù, *ACS Photonics* **2018**, *5*, 1779.
- [22] K. Wang, J. G. Titchener, S. S. Kruk, L. Xu, H.-P. Chung, M. Parry, I. I. Kravchenko, Y.-H. Chen, A. S. Solntsev, Y. S. Kivshar, *Science* **2018**, *361*, 1104.

- [23] N. A. Rubin, G. D'Aversa, P. Chevalier, Z. Shi, W. T. Chen, F. Capasso, *Science* **2019**, 365, eaax1839.
- [24] A. Pors, M. G. Nielsen, S. I. Bozhevolnyi, *Optica* **2015**, 2, 716.
- [25] Y. Ni, S. Chen, Y. Wang, Q. Tan, S. Xiao, Y. Yang, *Nano Lett.* **2020**, 20, 6719.
- [26] T. Lei, M. Zhang, Y. Li, P. Jia, G. N. Liu, X. Xu, Z. Li, C. Min, J. Lin, C. Yu, *Light: Sci. Appl.* **2015**, 4, e257.
- [27] J. Zhou, H. Qian, C.-F. Chen, L. Chen, Z. Liu, *Nano Lett.* **2020**, 21, 330.
- [28] G. Zheng, H. Mühlenbernd, M. Kenney, G. Li, T. Zentgraf, S. Zhang, *Nat. Nanotechnol.* **2015**, 10, 308.
- [29] Z. Lin, X. Li, R. Zhao, X. Song, Y. Wang, L. Huang, *Nanophotonics* **2019**, 8, 1079.
- [30] J. Wen, L. Chen, B. Yu, J. B. Nieder, S. Zhuang, D. Zhang, D. Lei, *ACS Nano* **2021**, 15, 1030.
- [31] S. Lei, X. Zhang, S. Zhu, G. Geng, X. Li, J. Li, Y. Wang, X. Li, L. Huang, *Opt. Express* **2021**, 29, 18781.
- [32] L. Huang, X. Song, B. Reineke, T. Li, X. Li, J. Liu, S. Zhang, Y. Wang, T. Zentgraf, *ACS Photonics* **2017**, 4, 338.
- [33] C. Spägele, M. Tamagnone, D. Kazakov, M. Ossiander, M. Piccardo, F. Capasso, *Nat. Commun.* **2021**, 12, 3787.
- [34] A. A. Cuyt, V. Petersen, B. Verdonk, H. Waadeland, W. B. Jones, *Handbook of Continued Fractions for Special Functions*, Springer, Berlin, Germany **2008**.
- [35] A. Georgiou, J. Christmas, N. Collings, J. Moore, W. Crossland, *J. Opt. A: Pure Appl. Opt.* **2008**, 10, 035302.
- [36] C. Tao, C. Tao, *The Theory of Optical Information*, Science Press, Beijing, China **2005**.
- [37] C. J. Sheppard, K. G. Larkin, *Optik* **2003**, 113, 548.
- [38] I. Cox, C. Sheppard, *J. Opt. Soc. Am. A* **1986**, 3, 1152.
- [39] R. Zhao, L. Huang, Y. Wang, *Photonix* **2020**, 1, 20.
- [40] J. Sung, G. Y. Lee, C. Choi, J. Hong, B. Lee, *Adv. Opt. Mater.* **2019**, 7, 1801748.